Digitised Optimisation of Nanoparticle Synthesis via Laser Ablation: An Industry 4.0 Multivariate Approach for Enhanced Production

Brian Freeland [1,2,*], Ronan McCann [3], Burcu Akkoyunlu [2], Manuel Tiefenthaler [1,4], Michal Dabros [4], Mandy Juillerat [4], Keith D. Rochfort [2], Greg Foley [2] and Dermot Brabazon [1]

1   I-Form Advanced Manufacturing Research Centre, Dublin City University, Glasnevin,
    D09 V209 Dublin, Ireland
2   School of Biotechnology, Dublin City University, Glasnevin, D09 V209 Dublin, Ireland;
    keith.rochfort@dcu.ie (K.D.R.)
3   School of Science and Computing, South East Technological University, X91 Waterford, Ireland
4   School of Engineering and Architecture HES-SO, University of Applied Sciences and Arts Western
    Switzerland, Bd de Pérolles 80, CH-1700 Fribourg, Switzerland; michal.dabros@hefr.ch (M.D.);
    juilleratmandy@hotmail.com (M.J.)
*   Correspondence: brian.freeland@dcu.ie

Abstract: The synthesis of nanoparticles (NPs) via laser ablation synthesis in solution (LASiS) is a promising method for sustainable and efficient nanoparticle fabrication. This work investigates the transition from one-factor-at-a-time experimentation to a more efficient, multivariate approach for optimising NP production efficiency. By applying the Industry 4.0 principles, the objective is to digitise and automate laboratory processes to increase productivity and robustness. Design of Experiments (DoE) strategies, Taguchi orthogonal arrays and full-factorial design (FFD), have been employed to enhance laser ablation processes. Both models confirmed that increasing laser power led to higher colloid absorbance, with the Taguchi DoE offering rapid initial process mapping and FFD providing a higher-resolution analysis. The optimal laser repetition rate of 30 kHz was identified as a balance between pulse energy and thermal effects on the target, maximising ablation efficiency. The Taguchi model had a prediction of NP size with an R^2 value of 0.49, while the FFD struggled with accurate size prediction. Additionally, this study introduced a recirculation flow regime as a rapid test platform for predicting optimal conditions for continuous flow production. Using a semi-autonomous DoE platform decreased the operator involvement and increased the process selectivity. This proof-of-concept for on-the-bench NP rapid manufacturing demonstrated how efficient NP synthesis processes can be developed by clarifying the effects of varying parameters on colloid productivity, paving the way for broader industrial applications in the future.

Keywords: nanoparticles; laser ablation synthesis in solution; silicon nanoparticles; additive manufacturing; design of experiments; automation; Industry 4.0; material processing

1. Introduction

With the increasing demand for nanoparticles (NPs), physical synthesis methods such as laser ablation synthesis in solution (LASiS) have gained significant attention over the years. Compared to traditional chemical synthesis methods, LASiS produces ligand-free NPs, and it is an environmentally safer option since no harmful solvents are required [1–3].

The LASiS technique operates by focusing a high-energy laser beam onto a solid target submerged in a liquid medium. This interaction leads to the formation of a plasma plume, which rapidly cools and condenses to form NPs. The size, shape, and properties of the NPs can be finely tuned by adjusting laser parameters such as repetition rate, pulse duration, as well as the characteristics of the surrounding liquid. In addition, this technique facilitates various single-step post-production functionalization, expanding their applicability in fields like chemical separation, biosensing, cellular labelling, and display technologies. Despite these advancements, scale-up and transitioning from batch to continuous production remain as key challenges for this technique to compete commercially with wet-chemical production methods.

Synthesis of nanoparticles is a multivariate process requiring considerable testing to determine the critical process parameters (CPPs) required for process optimisation. The digitisation of processes, such as LASiS for NP production, aids in achieving wide-scale adoption in the mass market. The digitisation of experimental data allows for insights at process, batch, and laboratory levels. On a laboratory scale, digitisation along the lines of Industry 4.0 allows for manufacturing research and development testbeds to achieve higher productivity. Industry 4.0 architecture integrates artificial intelligence and cloud computing to create smart, adaptive production systems. They emphasise real-time data, scalability, and interoperability for efficient and sustainable operations [4]. The integration and automation of process analytics reduces experimental time by eliminating many tasks which must be manually performed otherwise. This can also have the added benefit of reducing operator error, increasing the reliability of the collected data. Through implementing these Industry 4.0 architectures at the research and development stage, the potential obstacles can be minimised for the adoption of new technologies in industries, which LASiS could benefit from. Design of Experiments (DoE) strategies have been used extensively to optimise laser ablation processes [5]. Previously, Taguchi-based designs have been implemented to optimise laser conditions, such as the ablation of cyclic olefin polymer (COP) targets [6]. Loutas et al. utilised full-factorial and box-Behnken DoE strategies to investigate the interaction of laser parameters with surface topologies and bonding strength of laminar polymers [7]. DoE has been applied to optimise pulsed-laser deposition of lead zirconate titanate on thin films [8]. Recently, DoE has been used toward process map generation for nanoparticle fabrication techniques. Khan et al. applied Taguchi orthogonal arrays to investigate the solvent chemistry parameter effect on the aggregation of ZnO NPs, applying response data attained from UV–Vis and FTIR spectroscopies [9]. Plackett–Burman and Taguchi designs were applied to optimise ZnO production via biosynthesis [10]. Full-factorial designs have been implemented to increase the stability and quality of solid lipid NPs [11] and to optimise PLGA/drug formulation to improve the treatment of tumours.

This work focuses on developing LASiS, constituted one factor at a time (OFAT) experimentation to gain process understanding towards optimising NPs production efficiency [2,12,13]. The research outlined in this paper transitions from single-factor testing towards a more efficient, multi-parameter-based design of experiments approach, and a new autonomous rapid technique is presented for characterising and producing NPs at an optimised production rate. The effects of laser parameters, such as fluence, repetition rate, and laser beam scan speed, are examined along with liquid conditions, including solvent flow rate and pressure. Initial experiments were carried out using a Taguchi orthogonal DoE to quickly develop a model towards optimisation of the design space and recommend optimum parameters for NP production, followed on by a reduced parameter, higher-resolution full-factorial design (FFD) of a smaller design space. The models were developed with the aim of examining the interaction effects of process parameters on NP ablation efficiency and colloid size dispersion to predict optimum process conditions. By

incorporating multi-parameter DoE and digitisation, this research aims to optimise the production efficiency of NPs, paving the way for a broader industrial adoption.

2. Materials and Methods

2.1. Experimental Setup

Silicon nano-colloids were produced using a "recirculatory" or "semi-batch" LASiS technique, introduced previously [2,12]. The process was adapted for automated production, as illustrated in Figure 1. The laser system used in this work was a picosecond-pulsed WEDGE HF 1064 (BrightSolutions, Prado, Italy) Nd:YAG laser with a wavelength of 1064 nm and a maximum pulse energy (E_p) of 147 µJ at 10 kHz, reducing to 50 µJ at 70 kHz pulse repetition frequency (f_{PRF}). The pulse duration (τ_p) increases linearly from 700 ps at 10 kHz to 2096 ps at 70 kHz PRF. The beam position and scan speed were controlled by a 2D scanning galvanometer (Raylase SS-12, (E-2)); the target was maintained within the beam waist via a 1D-nanopositioning stage (M-404 4PD, PI, Karlsruhe, Germany). The automated system composed of solvent reservoir, PTFE piping loop (88 mL internal volume), 3D printed NPs flow reactor, remotely actuated peristaltic pump (Isamatic MCPV510, Millipore Ltd., Burlington, MA, USA), remotely controlled solenoid valves, and at-line process analytical analysers (DLS, UV–Vis). For automated testing, the process variables (laser fluence, laser repetition rate, beam scan-speed, solvent pressure, and solvent flowrate) were controlled. Two process responses, namely UV–Vis absorbance and DLS NPs size distribution were monitored at-line. UV–Vis absorption was inferred as an indirect measurement of the concentration of the NP colloid fabricated. Test sequencing, machine control, and data acquisition were performed via an in-house-developed LabVIEW (National Instruments Inc., Austin, TX, USA) programme, the system was developed in alignment with Industry 4.0 principles as outlined in Figure 2, where ther is a flow of information from individual equipment (level 0) right through to cloud-based automation and scheduling (level 4). An ablation time of five minutes was chosen for all tests, allowing for an adequately dense colloid to be fabricated, meeting the limit of detection requirements of the at-line measurement devices, and removing the requirement for post-production concentration step [14] prior to colloid analysis. The short test time was expected to reduce the interaction effects of NPs occlusion and NP photo fragmentation [15], keeping the process as similar as possible to continuous flow production. The re-circulation mode continuously mixed the DLS by-pass loop with the main line, ensuring the colloid was homogenous in the system, and hence the measurement was representative of the bulk process fluid.
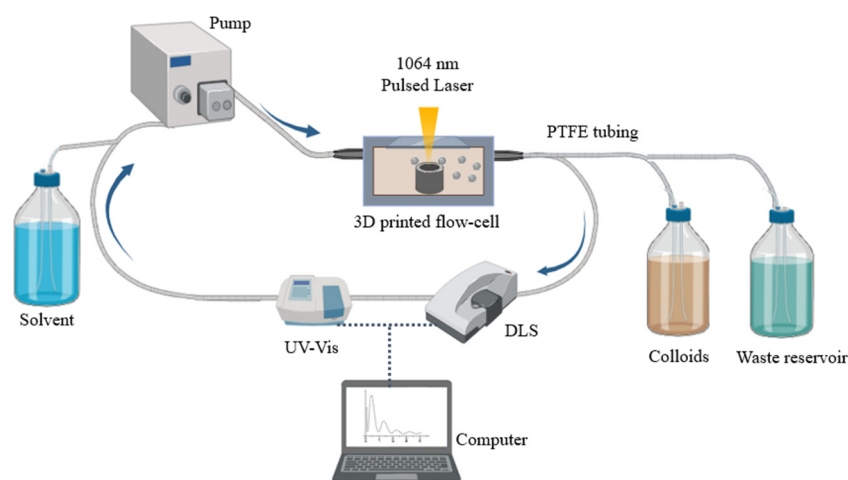

Figure 1. Experimental setup for ablation test spirals on Silicon disc targets using 1064 nm laser, flow cell reactor, at-line DLS, and UV–Vis.
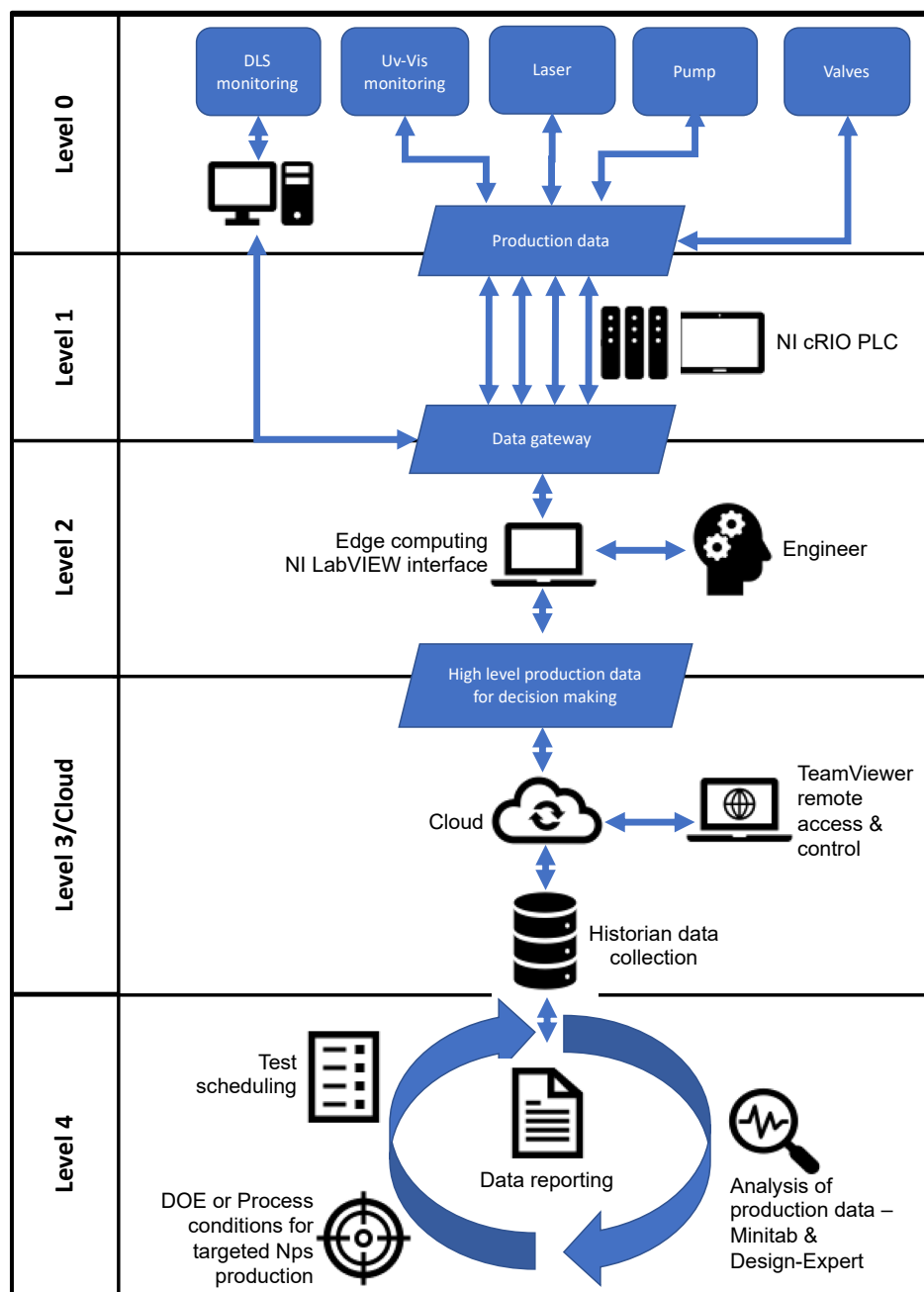
Figure 2. Industry 4.0 illustration of data transfer through the automated NPs manufacture rig.

2.2. Target Preparation

Silicon rods (8.28 mm diameter, 99.998% metals basis; Alfa Aesar, Heysham, UK) were cut (6 mm thickness) and mechanically polished (400 grade silicon carbide emery sheets) prior to testing. To allow for rapid characterisation, seven tests were performed on each target by ablating an Archimedean spiral (3 mm O.D., line spacing 100 μm) representing each individual test run, as shown in Figure 1. From prior testing, it was determined that under maximum operational laser fluence for 5 min ablation, the deepest 3 mm diameter ablation crater would be 0.64 mm, which is within the optimal beam width range for the laser optics.

2.3. Nanoparticle Colloid Characterisation

UV–Vis absorption spectroscopy was performed at-line and off-line, using a Libra S22 (Biochrom Ltd., Cambridge, UK), and was used to determine the ablation rate during

testing, since absorption correlates linearly with colloid concentration [1]. Thus, ablation rate can be inferred from the colloid concentration achieved. Gravimetrical-based ablated mass measurements were not possible as the target was not removed after each spiral ablation. Ablation crater volume and surface topologies were characterised using 3D optical profilometry (VHX-2000; Keyence, Osaka, Japan). A scan was performed upwards from the base of the ablation crater in 1 μm increments at a $500\times$ magnification, providing a direct measurement of ablated volume from which mass can be calculated from the known material density. Nanoparticle colloid size dispersion was monitored at-line and off-line via dynamic light scattering (DLS; Nanoflex, Microtrac Inc., York, PA, USA). Additional particle morphology measurement was performed off-line using an FEI Titan with field emission gun and spherical aberration corrector system (Cs-corrector) of the objective lens operated at 300 kV. TEM analysis was performed using a copper mesh TEM grid with 40 μL of sample applied and allowed to evaporate at room temperature.

2.4. Test Scheduling

The experiments ran semi-autonomously with manual interaction required to load each target. Set the flow-cell pressure and ablation site location. The total experimental run time for the 7 spirals on each target, including results acquisition and analysis, was under 140 min. The test sequencing is described in the Supplementary Material (Figure S2).

2.5. Model Development

The DoE arrays were produced and analysed using Design-Expert, version 7 (Stat-Ease Inc., Minneapolis, MN, USA) and Minitab 19 (Minitab LLC, State College, PA, USA) software. The minimum operational fluence (F_t) was chosen to be above the ablation threshold (F_{th}) for a silicon target reported previously (0.28 J/cm^2) for the experimental laser system used [16]. A command laser power (LP) of 61% laser power at 10 kHz repetition rate equates to 1.05 J/cm^2 and 0.62 J/cm^2 at 70 kHz repetition rate (RR). A scan speed test range was defined from 2 to 8 mm/s. Solvent gauge pressure values were selected within the working limits of the NP flow-cell. A range for solvent flow rates was selected from 15 to 240 mL/min, to reflect those reported in the literature [2,16,17]. Given that the experiments were run in recirculation mode, increasing the flow rate would not have a diluting effect on the colloids produced.

2.5.1. Taguchi Orthogonal Array

The experimental design chosen for the screening experiments was a Taguchi orthogonal array L_{16} consisting of five factors over four levels, detailed in Table 1. FR is the liquid flowrate, P is the liquid pressure (bar), LP is the command laser power (%), RR is the laser repetition rate (kHz), and SS the scan speed (mm/s). The test layout on the silicon targets is illustrated in Supplementary Material (Figure S1). Three replicates (R1–R3) were added to the Taguchi design, with one test allocated to each target to ensure inter-target normality. Validation tests (V1–V6) were performed within the design space, and model process optimisation tests were performed in triplicate (T1–T3). The full DoE is described in Table 2.

A reduced two-factor-interaction (2FI) model was developed for NP colloid absorbance prediction (and hence colloid concentration prediction) using a stepwise backward elimination to remove insignificant terms. The backward elimination would reduce model complexity while increasing the predicted coefficient of determination (R^2). The successful adoption of a 2FI model may indicate that only linear interactions between the parameters were observed; i.e., the parameters do not reach maxima points within the range chosen. However, caution must be taken with this assumption, as Taguchi models may alias small local maxima within the process space. Similarly, a 2FI model was developed for NP size

prediction, including the same backward elimination. A linear model was developed for the filtered colloid NP size estimation.

Table 1. Process parameters and levels for Taguchi orthogonal array.

Factors	Symbol	Unit	Level −2	Level −1	Level +1	Level +2	R
Laser power	LP	[%]	61	74.5	87	100	87
Repetition rate	RR	[KHz]	10	30	50	70	10
Scan-speed	SS	[mm/s]	2	4	6	8	2
Flow rate	FR	[ml/min]	15	90	165	240	165
Solvent pressure	P	[bar]	1	1.7	2.3	3	1

Table 2. FF reduced design space process parameters and levels.

Factors	Symbol	Unit	Level −1	Level 0	Level +1	R
Laser power	LP	%	70	80	100	80
Repetition rate	RR	kHz	10	35	60	35
Scan-speed	SS	mm/s	1.8	4.8	7.8	4.8

2.5.2. Full-Factorial Design

A higher-resolution full-factorial design (FFD) was developed to gain a greater understanding of the process interactions and increase the model accuracy within the previously examined process space. Solvent flow rate and pressure were removed as process variables to simplify the design space. Liquid flow rate was maintained at 180 mL/min and 2 bar gauge pressure. Based on the parameters described in Table 2, a reduced quadratic model was developed for colloid absorbance using backward elimination.

3. Results

3.1. Taguchi Model

The Taguchi DoE results, including colloid absorption and NPs size measurements, are documented in Table 3. A selection of the colloids produced can be seen in Figure 3, showing a range of process responses. The colloid absorbance reported in Table 3 ranged from a minimum value of 0.000 A.U. to a maximum of 0.360 A.U. with a mean value of 0.17 A.U., indicating a large spread in the process response. The at-line-measured Np sizes produced ranged from a minimum particle diameter of 125 nm to a maximum diameter of 327 nm with a process mean of 232 nm. Off-line post-filtration (0.2 μ) measurements yielded smaller NPs ranging from 6.8 nm to 77.3 nm with a mean size of 49 nm, indicating that smaller particles can be recovered from the colloids after filtration.

Figure 4 shows optical micrographs of the ablation targets and the range of surface topologies produced with various laser and process parameters, as determined by the Taguchi DoE. Low laser power (level −2 and −1) combined with average repetition rates (level 1) or medium to high scan speeds (level +1, +2) produced only faint surface ablations (Tests 3, 7, 12), indicating that the process was operating just above the ablation threshold. Repetition rates of 30 kHz and 50 kHz produced significant melt on the target surface (spiral #: 2 and 6), as these craters are deep relative to other tests, which implies that heating is aiding reducing the ablation threshold of the Si target. Replicates (R1–R3) display similar surface topologies, with each ablation spiral visible, as seen in Figure 4. They possessed an average crater depth of 239 ± 27 μm, equating to an ablated mass of 2.1 mg ± 0.25 mg for the 5 min ablation, indicating a target process variability of 12.8%.

Table 3. Taguchi orthogonal array, including replicate tests.

Label [-]	Run [-]	FR [ml/min]	P [bar]	LP [%]	RR [kHz]	SS [mm/s]	UV–Vis Abs @ 400 nm [A.U]	Np Size [nm]	Np Size (Filt.) [nm]
1	1	−2	+2	+2	+2	+2	0.075	232	29
2	2	+2	−2	+2	−1	1	0.330	257	52.7
3	3	+2	+2	−2	+1	−1	0.014	166	32.4
4	4	+1	−2	+1	+2	−1	0.018	161	53.8
5	5	+1	+1	−2	−1	+2	0.074	200	55.1
6	6	+1	−1	+2	+1	−2	0.245	242	47.6
R1	7	+1	−2	+1	−2	−2	0.286	212	52.5
7	8	+2	+1	−1	+2	−2	0.004	171	55
8	9	−2	+1	+1	+1	+1	0.010	193	50.9
9	10	−1	−2	−1	+1	+2	0.012	188	51
10	11	+1	+2	−1	−2	+1	0.265	325	52.5
11	12	−1	+2	+1	−1	−2	0.360	309	67.2
12	13	−1	−1	−2	+2	+1	0.000	327	40.2
R2	14	+1	−2	+1	−2	−2	0.296	275	74.8
13	15	−1	+1	+2	−2	−1	0.332	251	43.3
14	16	+2	−1	+1	−2	+2	0.319	125	46.3
15	17	−2	−2	−2	−2	−2	0.142	268	6.8
16	18	−2	−1	−1	−1	−1	0.050	226	77.3
R3	19	+1	−2	+1	−2	−2	0.305	292	49
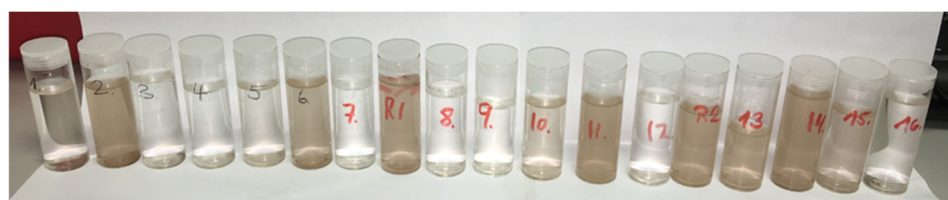
Figure 3. Colloids produced directed by the Taguchi screening model.

3.1.1. Signal-to-Noise Analysis

The signal-to-noise (S/N) ratio was determined to define the most significant factors in the Taguchi model. Semiconductor and bioanalytical research require a high volume of uniform sized SiNPs [18,19]. Therefore, two S/N ratios were chosen for this work, firstly to maximise the colloid concentration produced (absorbance) and secondly to minimise the nanoparticle size. Equations (1) and (2) describe the S/N definitions used for colloid absorbance and NPs size, respectively.

$$(\text{S}/\text{N})_{\text{Absorbance}} = -10\log_{10}\left(\Sigma\frac{1/z^2}{n}\right) \tag{1}$$

$$-(\text{S}/\text{N})_{\text{NPs size}} = -10\log_{10}\left(\Sigma\frac{y^2}{n}\right) \tag{2}$$

where z is the UV–Vis absorption, y is defined as the nanoparticle size, and n is the number of responses. Table 4 describes the calculated S/N ratios for the Taguchi experimental design for both colloid absorbance and NPs size response variables. The factors are ranked in terms of a "delta value", which is a calculation of the difference between the process response variables to the factor at level −2 and level 2. For the experimental range, the first-ranked factor was repetition rate, which possessed the highest delta value for both colloid absorbance and NPs size. The second-ranked factor was laser power for both responses, followed by laser scan speed. Liquid pressure had the smallest effect on the change in process responses in the range used.
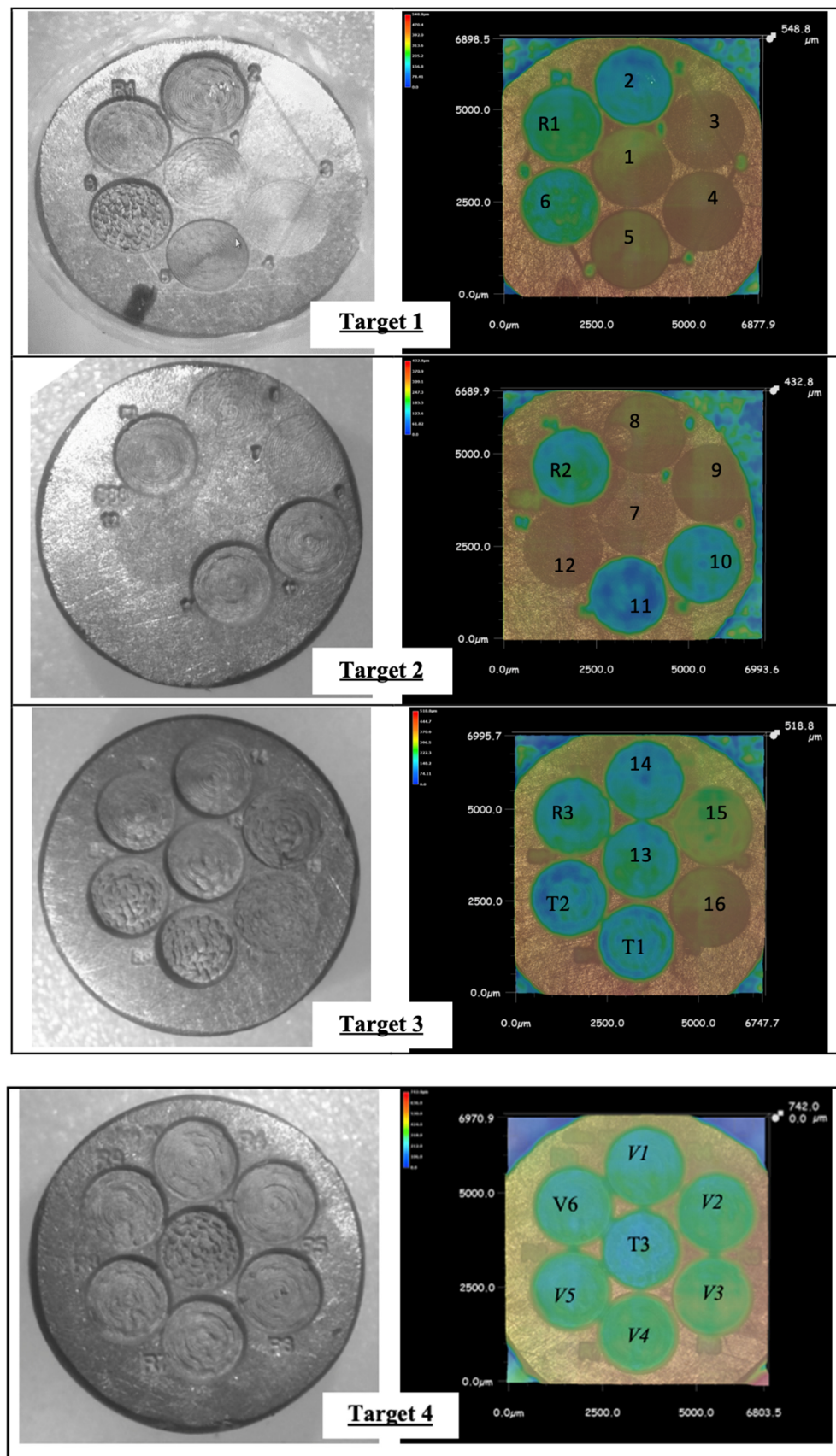
Figure 4. Taguchi DOE target surface ablation showing: target 1 (1–6, R1), target 2 (7–12, R2), target 3 (13–16, R3, R4, T1, T2), and target 4 (T3, R4–R9) taguchi DOE target surface ablations.

Table 4. Responses for signal-to-noise ratio of colloid absorbance and NPs size for Taguchi test.

Response	Factor	Level				Delta	Rank
		−2	−1	1	2		
Colloid absorbance	RR	−12	−16.78	−32.02	−46.11	34.11	1
	LP	−38.77	−31.24	−23.42	−13.48	25.29	2
	FR	−26.37	−33.91	−20.32	−26.32	13.6	3
	SS	−21.67	−26.89	−34.9	−23.46	13.23	4
	P	−25.07	−31.64	−30.21	−20	11.65	5
NPs size	RR	−40.15	−41.36	−40.04	−35.77	5.59	1
	LP	−38.45	−41.9	−36.43	−40.54	5.47	2
	FR	−38.89	−41.41	−40.51	−36.51	4.91	3
	SS	−41.68	−38.36	−39.61	−37.67	4.01	4
	P	−37.89	−39.92	−38.37	−41.15	3.26	5

From the main effects plots illustrated in Figures 5 and 6, it can be concluded that linear trends exist between laser power, repetition rate, and the absorbance signal-to-noise ratio. Increasing laser power and reducing repetition rate will directly increase the signal-to-noise ratio. This observation agrees with general research where increasing laser pulse energy will increase NPs productivity [1,18,20,21]; as for the experimental laser system used, increasing the repetition rate has the effect of reducing the pulse energy supplied to the target. It is more difficult to determine clear trends for the NPs size signal-to-noise ratio. At repetition rates above 30 kHz and 90 mL/min solvent flowrate, a trend is observed towards reducing the NP-size signal-to-noise ratio, indicating that lower pulse energies with increased reirradiation may produce smaller NPs.
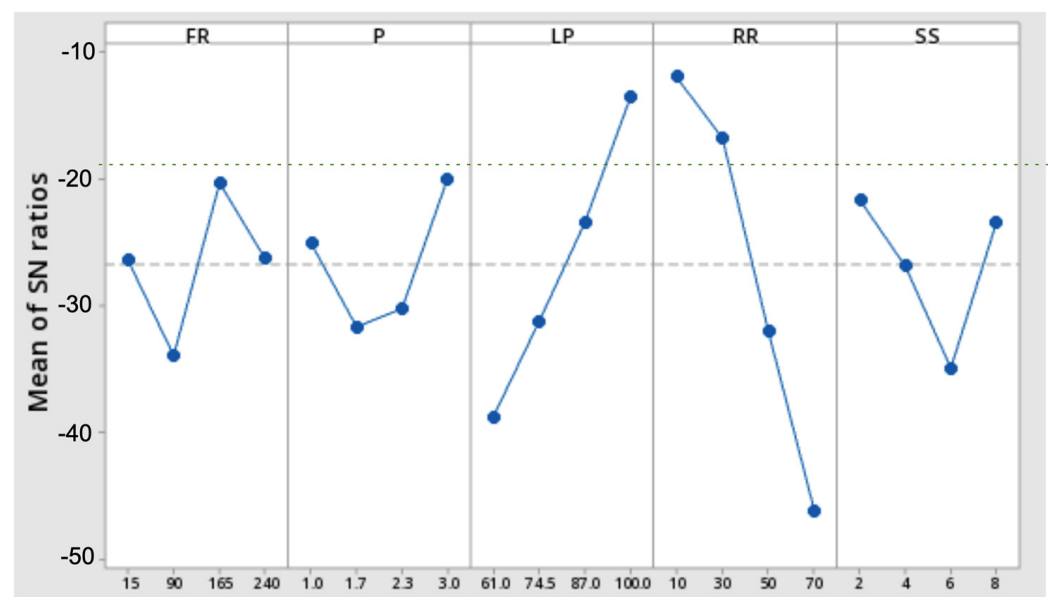
Figure 5. Main effects plots for S/N ratios of data means for colloid absorbance, dotted line represents the overall mean of SN ratios.

3.1.2. ANOVA Analysis
Colloid Absorbance

Table 5 indicates the primary analysis of variance (ANOVA) parameters sourced from the Taguchi colloid absorbance model developed. The absorption model had an adjusted R^2 of 0.92, which was within agreement of the predicted R^2 of 0.83.
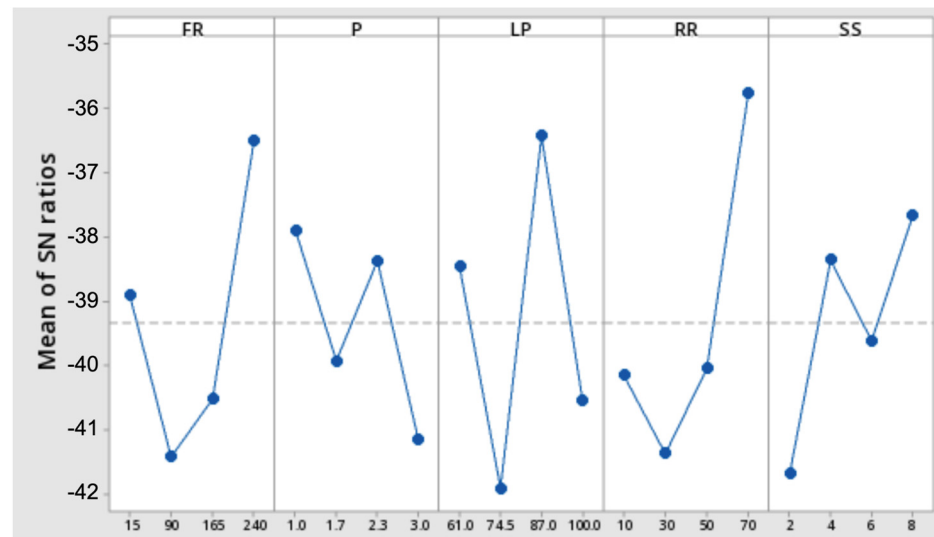
Figure 6. Main effects plots for S/N ratios of data means for NPs size, dotted line represents the overall mean of SN ratios.

Table 5. Responses for signal-to-noise ratio of colloid absorbance and NPs size for Taguchi test.

Response	DoF	Adjusted R^2	Predicted R^2	Adequate Precision	F Value
Absorbance units (A.U)	7	0.92	0.83	16.20	31.25

The adequate precision of the absorbance model was 16.20; i.e., the signal-to-noise ratio was large (>4), indicating that noise is not a significant factor in the model. The F-value, which compares the model variance to the residual variance (31.25), showed that the model is significant. The Equation derived using the Design Expert Software to predict absorbance is as follows:

$$Abs. (A.U.) = (0.594 - \left(5.577 \times 10^{-3} \times FR\right) + (0.130 \times P) - \left(2.71 \times 10^{-3} \times LP\right) - (0.011 \times RR)$$
$$- (0.045 \times SS) + \left(8.04 \times 10^{-5} \times FR \times LP\right) + \left(1.09 \times 10^{-3} \times RR \times SS\right))^2 \tag{3}$$

where Abs is the colloid UV–Vis spectra absorbance in (A.U.). The model derived was complex, containing 12 factors and 12 degrees of freedom (DoF). This complex behaviour is expected, as many interactions between the variables contribute to colloid production. It was seen that increasing RR had a negative effect on concentration; this result was expected as the pulse energy drops with RR for the experimental laser system. Scan speed had the lowest impact on the system, with a slight reduction in concentration observed with increasing speeds. The linear behaviour of the model is unexpected due to the inherent non-linearity documented for laser processes [22]; however, as discussed previously, this observed linearity indicates that the saturation response of the variables due to process conditions such as photo fragmentation and particle occlusion of target with no melting observed. The normality of the dataset was determined using a residuals plot as illustrated in the Supplementary Material (Figure S4), showing random variation in absorbance over the tests performed. This indicated that replacing the target had no significant effect on the process. A linear correlation of model prediction vs. experimental data was also observed (Figure S5 in Supplementary Material) for colloid absorbance, indicating that the model is capable within the design space.

The surface plots illustrated in Figure 7 show the linear relationship between the input parameters and absorption; this would indicate that the Taguchi model does not offer high

enough resolution to model the interaction effects, or that no process local maxima were reached within the design space chosen.
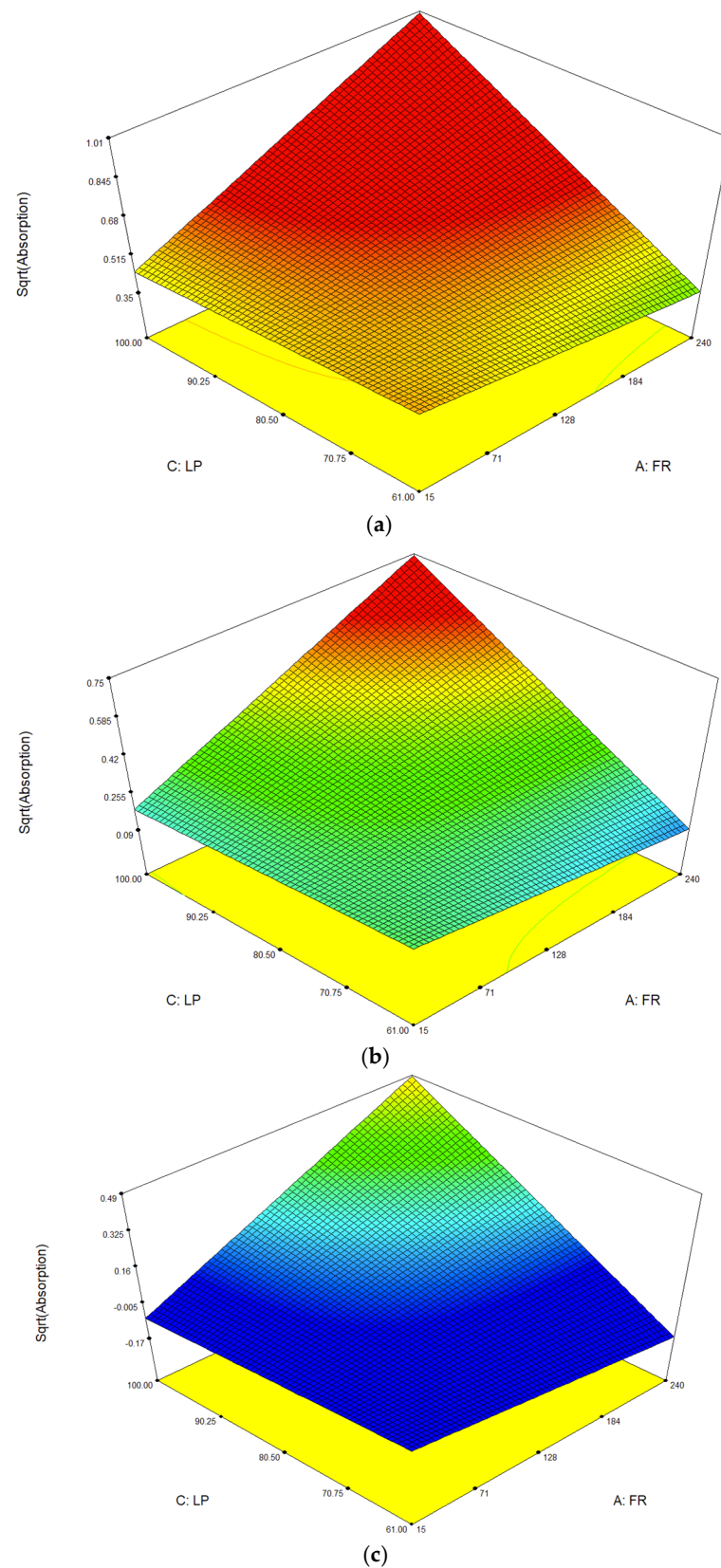

Figure 7. Surface plots of the effect of Laser command power (%) and liquid flowrate on colloid absorption for repetition rates at (**a**) 10 kHz, (**b**) 30 kHz, and (**c**) 70 kHz, the colours indicate low absorption(blue), medium(green & yellow), increasing to high (red).

Nanoparticle Diameter

Table 6 indicates the primary analysis of variance (ANOVA) parameters sourced from the Taguchi NPs size model developed. The NP size model developed was statistically significant, with an F-value of 7.71. The predicted R^2 of 0.49 is not as close to the adjusted R^2 value of 0.75 to traditionally describe the model as being precise. The difference between the adjusted R^2 and the predicted R^2 for nanoparticle size was greater than 0.2, indicating that the model required more training data to describe the process correctly.

Table 6. Responses for signal-to-noise ratio of colloid absorbance and NPs size for Taguchi test.

Response	DoF	Adjusted R^2	Predicted R^2	Adequate Precision	F Value
NPs size (nm)	8	0.75	0.49	10.75	7.71
Filtered NPs size (nm)	3	0.31	0.17	5.77	1.07

The adequate precision value of 10.75 indicated that noise is not a significant factor. The residuals chart (Supplementary Material Figure S6) shows that the process was under control and contained no systematic errors. The model predicted vs. actual plot in the Supplementary Material (Figure S7) determines that there is a linear correlation with experimental data. The model developed containing 8 degrees of freedom is described below:

$$NP\ size\ (nm) = 718.850 - (4.131 \times FR) + (165.901 \times P) - (6.795 \times LP) - (4.340 \times RR) - (63.467 \times SS)$$
$$+ (0.055 \times FR \times LP) - (2.240 \times P \times RR) + (1.717 \times RR \times SS) \tag{4}$$

The model developed using the filtered colloid NP size data was not statistically significant, possessing an F-value <4, (1.07). The model performance was low, with an R^2 of 0.31, and the adequate precisions proved that noise was not a determining factor in the model. This result shows that with a limited number of data points, the Taguchi models struggled to determine a relationship between process variables and NPs size. The NP size response only varied by 25% from the mean value for the runs tested, indicating that perhaps a higher resolution DoE model would prove more successful.

3.1.3. Model Validation

In order to validate the absorbance model, independent verification tests were performed, and the model prediction was compared against experimental data, as described in Table 7. The model prediction performance was seen to be good with parameters on the edge of its design space (V1–V3) and with a mean relative error (MRE) of 6.5%. However, the model's interpolation accuracy was reduced, with an MRE of 30.9%, when tested against experimental data using parameters towards the centre of its design space (V4–V6). This alludes to a lack of resolution of the Taguchi DoE, where only linear variable interactions were found, along with no parameter process maxima points.

Table 7. Taguchi model testing and productivity maximum (*n* = 3).

Label [-]	FR [mL/min]	P [bar]	LP [%]	RR [kHz]	SS [mm/s]	Abs. Pred. [A.U.]	Abs. Exp [A.U.]	MRE [%]	Ablation Rate [mg/h]
Ver 1 (V1–V3)	199	1	92	25	6	0.25	0.327 ± 0.01	30.98	24.3 ± 3.9
Ver 2 (V4–V6)	101	2.4	100	10	4	0.36	0.337 ± 0.01	6.5	21.0 ± 0.2
Test$_{max}$ (T1-3)	188	2.5	100	24	2	0.44	0.372 ± 0.01	38.2	25.2 ± 2.5

Optimal process conditions were investigated by using Design Expert to solve for maximising the response in Equation (3) to achieve the highest possible colloid concentration. Afterwards, the model was solved to maximise the response, as described in Table 7. The absorbance target was set at 0.4 A.U., and the resulting experiment produced a colloid with an absorbance of 0.372 A.U., offering an MRE of 7% from experimental data. The prediction indicated higher colloid concentration produced than observed in the training dataset. Therefore, using the techniques, a higher colloid concentration was reached than previously determined for the process variables [2]. The model performed well when predicting absorbance close to the edge of the trained design space. It also offered a rapid method to reach process variables for optimised production.

The UV–Vis absorbance spectra of the colloid produced under optimum process conditions is illustrated in Figure 8a with a linear correlation between colloid concentration and absorbance at 400 nm determining colloid concentration (Figure 8b). TEM analysis (Figure 9a) showed that the NPs are spherical and DLS determined (Figure 9b) the colloid to have a peak diameter of 106 ± 65 nm. The SEM images (Figure 10) illustrate that heating of the target must contribute to increasing NPs production efficiency. Significant melt can be seen on the process optimum target (T3) compared with a target ablated with conditions towards the centre of the design space.
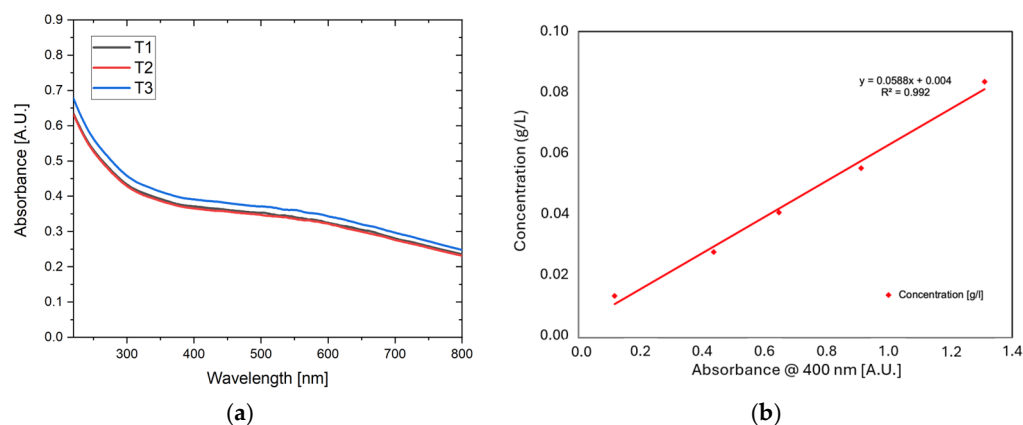

(a)

(b)

Figure 8. (**a**) UV–Vis absorption of triplicate process optimisation tests and (**b**) correlation of colloid concentration (C) to measured absorbance (A) at 400 nm, C = 0.0588 (A) + 0.004.
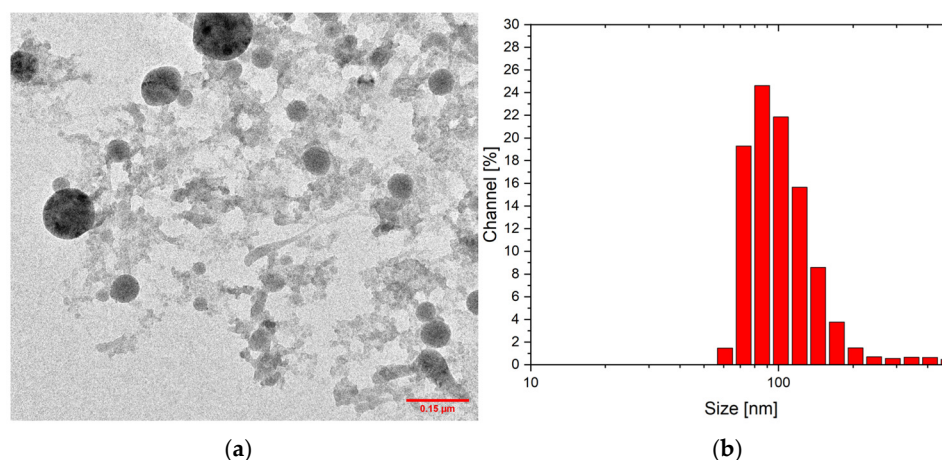

(a)

(b)

Figure 9. (**a**) TEM image of the colloid produced under optimised conditions and (**b**) DLS measurement showing a peak at 106 ± 65 nm.
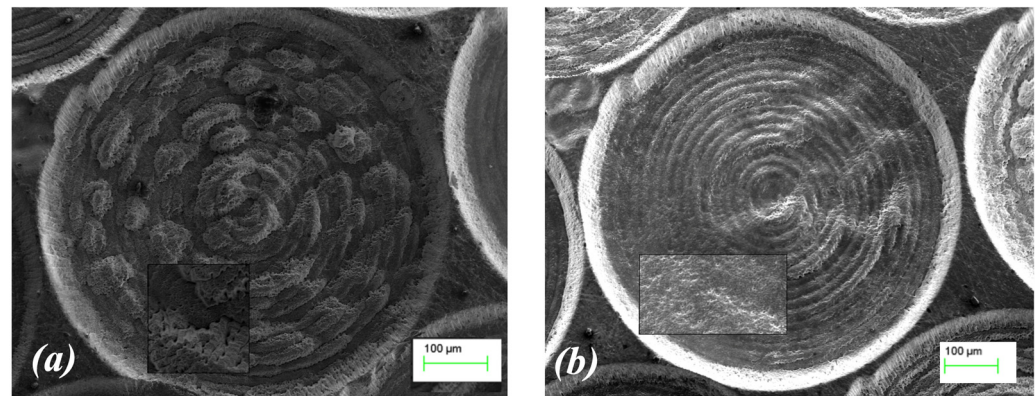
Figure 10. TEM (**a**) Sample T3 ablation spiral utilising optimised parameters as described in Table 7, SEM operating at 12.05 kV, WD = 8 mm and (**b**) spiral 13, produced via FR = 90 mL/min, P = 1.7 bar, F = 1.83 J/cm^2, RR = 10 kHz, SS = 4 mm/s, SEM operating at 13.53 kV, WD = 8.5.

3.2. Full-Factorial Model

The results for the FFD are documented in Table 8. The average absorbance measurement was 0.21 ± 0.11 A.U. A variation of 52% from the mean was produced within the dataset, indicating a reasonable spread of data. The NPs size data contained a similar range from the mean of 129 nm ± 62 nm.

Table 8. Full-factorial design experimental table and results.

Target [-]	Run [-]	LP [%]	SS [mm/s]	RR [kHz]	UV–Vis Abs @ 400 [-]	DLS Size [nm]
1	1	0	−1	0	0.2638	68.8
1	2	1	−1	0	0.3271	139.8
1	3	1	1	0	0.3474	129.7
1	4	1	0	−1	0.3196	88.6
1	5	−1	0	−1	0.2100	63.4
1	6	1	1	1	0.1687	174.2
1	7	0	0	0	0.2728	106.7
2	8	0	1	0	0.2802	36.1
2	9	−1	−1	−1	0.2921	117.1
2	10	0	0	−1	0.3157	122.3
2	11	−1	−1	1	0.0202	58.2
2	12	0	−1	1	0.0402	120.8
2	13	1	0	1	0.1589	253.2
2	14	1	1	−1	0.3132	123.0
3	15	0	0	0	0.2300	190.7
3	16	−1	0	1	0.0095	67.5
3	17	−1	1	0	0.1609	235.7
3	18	1	−1	−1	0.3079	110.0
3	19	1	0	0	0.3386	92.8
3	20	0	0	0	0.2974	113.3
4	21	−1	−1	0	0.1627	94.1
4	22	−1	0	0	0.1667	47.3
4	23	−1	1	1	0.0047	126.1
4	24	1	−1	1	0.1324	90.3
4	25	0	0	0	0.2714	212.8
4	26	0	0	1	0.0565	267.8
4	27	−1	1	−1	0.2571	243.2
5	28	0	1	1	0.0432	153.3
5	29	0	−1	−1	0.3259	95.7
5	30	0	1	−1	0.3113	136.0

ANOVA Analysis

A full-factorial design (FFD) was developed to more accurately map the process space bounds indicated from the Taguchi model. A quadratic model was developed via backward stepwise elimination with scan speed removed as a significant term. The final model equation possessed three degrees of freedom and is described in Equation (5):

$$A = -0.095 + \left(4.22 \times 10^{-3} \times LP\right) + \left(4.26 \times 10^{-3} \times RR\right) - \left(1.25 \times 10^{-4} \times RR^2\right) \quad (5)$$

The quadratic relationship of colloid concentration with repetition rate is illustrated in the response charts (Figure 11). The residuals chart for the tests conducted indicated that the process was within control at all times and is available in the ESI.
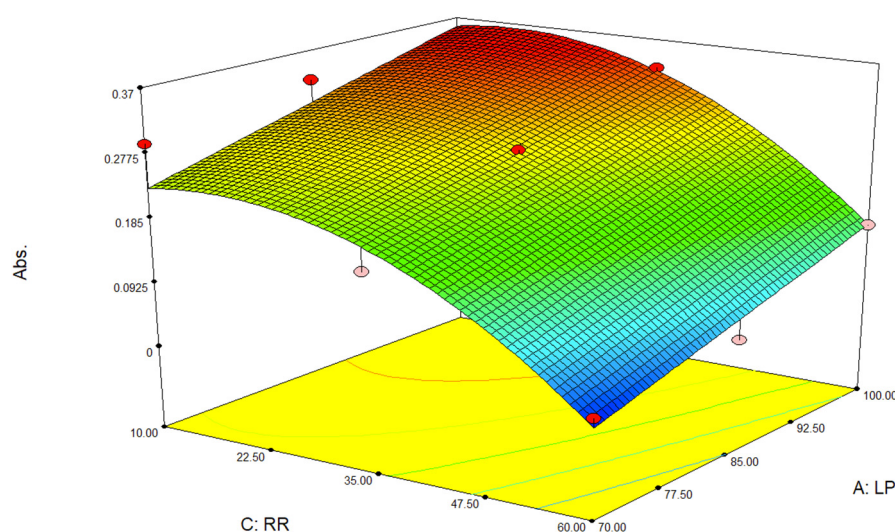

Figure 11. Response surface for colloid absorbance (A.U.) vs. laser repetition rate and laser command power with beam scan speed at 1.8 mm/s, red dots indicate the design points above prediction surface and pink dots represent design points below prediction surface.

The ANOVA parameters of the absorbance model developed via the full-factorial design (FFD) is described in Table 9. The model was seen to be significant, with an F-Value of 122.34, and the high adequate precision indicates that noise did not contribute significantly to the model. The model-predicted R^2 was within 0.02 of the adjusted R^2, indicating that the prediction represents the process space well.

Table 9. Full-factorial design experimental table and results.

Response	DoF	Adjusted R^2	Predicted R^2	Adequate Precision	F Value
Absorption (A.U)	3	0.926	0.910	31.48	122.34

4. Discussion

In this study, the process parameters for producing silicon nano-colloids were optimised using two experimental designs: a Taguchi orthogonal array and a full-factorial design (FFD). For the Taguchi design, five factors were varied across four levels: laser power (61–100%), repetition rate (10–70 kHz), scan speed (2–8 mm/s), solvent flow rate (15–240 mL/min), and solvent pressure (1–3 bar). The process optimisation was conducted using a 2FI model to predict NP colloid absorbance and size. A full-factorial model was developed to fully map the process space inside the bounds seen from the Taguchi model, where solvent flow rate and pressure were held constant (180 mL/min and 2 bar,

respectively). The laser power (70–100%), repetition rate (10–60 kHz), and scan speed (1.8–7.8 mm/s) were systematically varied to further refine the model and improve accuracy in predicting colloid absorbance and NP size. The full-factorial model was seen as a simpler alternative to the Taguchi model, having four less degrees of freedom. It should be noted however that the Taguchi had a fewer number of total experiments, thus highlighting the importance of lower-resolution experimental designs on initial process space mapping. The full-factorial model agreed with the generalised models for laser ablation processes, including LASiS, where an increase in incident laser power corresponds to an increase in the ablation rate (as measured in this case through colloid absorbance) [15].

The quadratic relationship of colloid absorbance with repetition rate (Figure 11) shows the existence of an optimum repetition rate, in this case 30 kHz. This is a function of the laser system used, where f_{PRF} is linked with τ_{p} and E_{p} and agrees with other ablation experimental work on similar laser systems [2,6,23]. For low f_{PRF}, there are higher pulse energies but shorter pulse widths, thus inducing less thermal energy in the target. As f_{PRF} increases, E_{p} decreases, but the longer pulse widths cause an increase in the target temperature at the ablation site, thus decreasing the effective ablation fluence threshold, $F_{\mathrm{th}}^{\mathrm{eff}}$. The f_{PRF} of 30 kHz represents the trade-off between decreasing $F_{\mathrm{th}}^{\mathrm{eff}}$ while keeping E_{p} (and therefore F) sufficiently high to maintain high ablation rates.

The Taguchi DoE employed in this test offered a rapid technique to examine the effects of process parameters on ablation efficiency. A wide range of colloid concentrations were produced, indicating a range of ablation rates, which suggests the possibility of promising results with future development. Results achieved from the Taguchi model were broadly in agreement with the full-factorial testing DoE performed. This confirms that the Taguchi model, coupled with the developed system-automated process parameter trialling, offers a rapid method to optimise the production process with a limited number of experiments required, correlating well with high-resolution experimentation. The Taguchi model lacks resolution to describe the non-linear interactions of the process; however, it was successful in optimising colloid concentration. Both models struggled to model NPs size. The Taguchi model offered a prediction model for NP size with a prediction R^2 of 0.49, whereas the FFD was unable to yield a description of NPs size based on the input parameters.

The automatic experimental rig worked satisfactorily where it performed the 16 DoE experiments in 5 h, requiring manual input only to change targets and automatically performed response monitoring, data logging, and analysis. The combination of a Taguchi model with the automatic rig allowed for the prediction of a process optima, providing time efficient results compared to requiring several months experimental time for the single-factor testing. The combination of the autonomous rig and DoE paves the way for future rapid experiments to characterise the NP synthesis process for many other materials.

5. Conclusions

This study demonstrated a successful multivariate approach to optimising nanoparticle (NP) synthesis via laser ablation synthesis in solution (LASiS) using Industry 4.0 principles. By digitising and automating the process and applying design of experiments (DoE) methodologies, particularly the Taguchi orthogonal array and full-factorial design (FFD), production efficiency was significantly enhanced, with a clearer understanding of key process parameters.

The Taguchi DoE efficiently explored a broad parameter space, revealing that laser repetition rate and power are critical for maximising NP concentration. However, it had limitations in modelling non-linear interactions, with moderate predictive accuracy for NP size (R^2 = 0.49). The FFD provided higher resolution, confirming a quadratic relationship between colloid concentration and repetition rate, with 30 kHz as the optimal frequency.

Similar to the Taguchi model, it struggled to predict NP size, suggesting the need for further refinement. The automated rig and DoE approach reduced experimental time while maintaining accuracy, demonstrating the potential for semi-autonomous nanoparticle manufacturing.

Further refinement of NP size modelling can be achieved by using lower-repetition-rate lasers (<1 kHz), adding salts [12,24] to the solvent to control nucleation and aggregation [25], and optimising solvent selection. The choice of solvent affects NP size through its impact on surface oxidation, viscosity, and cavitation bubble dynamics, all which influence particle size and distribution [26–29].

Supplementary Materials: The following supporting information can be downloaded at https://www.mdpi.com/article/10.3390/pr13020388/s1: Figure S1. Spiral placement on targets 1–4, for Taguchi DOE., Figure S2. Flow chart of semi-automatic DOE program, Table S1. Example of automatic experiment table loaded into the automatic LASiS test software, Figure S3. Full-factorial experiments target layout, Figure S4. Plot of residuals vs. run number for Taguchi colloid absorption modelling, Figure S5. Plot of model prediction vs experimental absorbance values (A.U.) for Taguchi 74 colloid absorption modelling, Figure S6. Chart of residuals vs. run number for at-line nano colloid size modelling, Figure S7. Plot of model predicted size vs. experimental size measurement and Figure S8. Chart of residuals vs. run number FFD colloid absorption modelling.

References

1. Barcikowski, S.; Amendola, V.; Marzun, G.; Rehbock, C.; Reichenberger, S.; Zhang, D.; Gökce, B. *Handbook of Laser Synthesis of Colloids*; DuEPublico: Duisburg-Essen, Germany, 2016.

2. Freeland, B.; McCann, R.; O'Neill, P.; Sreenilayam, S.P.; Tiefenthaler, M.; Dabros, M.; Juillerat, M.; Foley, G.; Brabazon, D. Real-time monitoring and control for high-efficiency autonomous laser fabrication of silicon nanoparticle colloids. *Int. J. Adv. Manuf. Technol.* **2021**, *114*, 291–304. [CrossRef]

3. Manikandan, N.A.; McCann, R.; Kakavas, D.; Rochfort, K.D.; Sreenilayam, S.P.; Alkan, G.; Stornetta, T.; McGivern, A.R.; Grintzalis, K.; Friedrich, B.; et al. Production of Silver Nano-Inks and Surface Coatings for Anti-Microbial Food Packaging and Its Ecological Impact. *Int. J. Mol. Sci.* **2023**, *24*, 5341. [CrossRef]

4. Tsaramirsis, G.; Kantaros, A.; Al-Darraji, I.; Piromalis, D.; Apostolopoulos, C.; Pavlopoulou, A.; Alrammal, M.; Ismail, Z.; Buhari, S.M.; Stojmenovic, M.; et al. A Modern Approach towards an Industry 4.0 Model: From Driving Technologies to Management. *J. Sens.* **2022**, *2022*, 5023011. [CrossRef]

5. Parmar, A.; Kapil, S.; Sachar, S.; Sharma, S. Design of experiment based methodical optimization and green syntheses of hybrid patchouli oil coated silver nanoparticles for enhanced antibacterial activity. *Curr. Res. Green Sustain. Chem.* **2020**, *3*, 1000016. [CrossRef]

6. McCann, R.; Bagga, K.; Duaux, G.; Stalcup, A.; Vázquez, M.; Brabazon, D. Taguchi method modelling of Nd:YAG laser ablation of microchannels on cyclic olefin polymer film. *Opt. Laser Technol.* **2018**, *106*, 265–271. [CrossRef]

7. Loutas, T.H.; Sotiriadis, G.; Tsonos, E.; Psarras, S.; Kostopoulos, V. Investigation of a pulsed laser ablation process for bonded repair purposes of CFRP composites via peel testing and a design-of-experiments approach. *Int. J. Adhes. Adhes.* **2019**, *95*, 102407. [CrossRef]

8. Schatz, A.; Pantel, D.; Hanemann, T. Application of DoE methods to establish a model for the pulsed laser deposition of PZT thin-films. In Proceedings of the 2016 Joint IEEE International Symposium on the Applications of Ferroelectrics, European Conference on Application of Polar Dielectrics, and Piezoelectric Force Microscopy Workshop (ISAF/ECAPD/PFM), Darmstadt, Germany, 21–25 August 2016.

9. Khan, R.; Inam, M.A.; Park, D.R.; Zam Zam, S.; Yeom, I.T. Taguchi Orthogonal Array Dataset for the Effect of Water Chemistry on Aggregation of ZnO Nanoparticles. *Data* **2018**, *3*, 21. [CrossRef]

10. El-Ghwas, D.E.; Mazeed, T.E.; El-Waseif, A.; Al-Zahrani, H.A.; Almaghrabi, O.A.; Elazzazy, A.M. Factorial Experimental Design for Optimization of Zinc Oxide Nanoparticle Production. *Curr. Nanosci.* **2020**, *16*, 51–61. [CrossRef]

11. Zielinska, A.; Ferreira, N.R.; Durazzo, A.; Lucarini, M.; Cicero, N.; Mamouni, S.E.; Silva, A.M.; Nowak, I.; Santini, A.; Souto, E.B. Development and Optimization of Alpha-Pinene-Loaded Solid Lipid Nanoparticles (SLN) Using Experimental Factorial Design and Dispersion Analysis. *Molecules* **2019**, *24*, 2683. [CrossRef]

12. Freeland, B.; McCann, R.; Alkan, G.; Friedrich, B.; Foley, G.; Brabazon, D. Stable nano-silver colloid production via Laser Ablation Synthesis in Solution (LASiS) under laminar recirculatory flow. *Adv. Mater. Process. Technol.* **2020**, *6*, 677–685. [CrossRef]

13. Balachandran, A.; Sreenilayam, S.P.; Madanan, K.; Thomas, S.; Brabazon, D. Nanoparticle production via laser ablation synthesis in solution method and printed electronic application- A brief review. *Results Eng.* **2022**, *16*, 100646. [CrossRef]

14. Khairani, I.Y.; Minguez-Vega, G.; Donate-Buendia, C.; Gokce, B. Green nanoparticle synthesis at scale: A perspective on overcoming the limits of pulsed laser ablation in liquids for high-throughput production. *Phys. Chem. Chem. Phys.* **2023**, *25*, 19380–19408. [CrossRef] [PubMed]

15. Intartaglia, R.; Bagga, K.; Brandi, F. Study on the productivity of silicon nanoparticles by picosecond laser ablation in water: Towards gram per hour yield. *Opt. Express.* **2014**, *22*, 3117–3127. [CrossRef] [PubMed]

16. Cannon, P.; Freeland, B.; Jaquiery, M.; McGlynn, E.; Gaughran, J. Single-step functionalization of silicon nanoparticles providing efficient DNA binding. *Colloids Surf. A Physicochem. Eng. Asp.* **2022**, *648*, 129217. [CrossRef]

17. Pavithran, S.S.; McCann, R.; McCarthy, E.; Freeland, B.; Fleischer, K.; Goodnick, S.; Bowden, S.; Honsberg, C.; Brabazon, D. Silver and Copper nano-colloid generation via Pulsed Laser Ablation in Liquid: Recirculation nanoparticle production mode. ESAFORM, ESAFORM. In Proceedings of the 24th International Conference on Material Forming, Liège, Belgique, 14–16 April 2021. [CrossRef]

18. Lopez, J.; Kling, R.; Torres, R.; Lidolff, A.; Delaigue, M.; Ricaud, S.; Hönninger, C.; Mottay, E. Comparison of picosecond and femtosecond laser ablation for surface engraving of metals and semiconductor. In Proceedings of the SPIE 8243, Laser Applications in Microelectronic and Optoelectronic Manufacturing (LAMOM) XVII, 8243, San Francisco, CA, USA, 23–26 January 2012.

19. Intartaglia, R.; Bagga, K.; Scotto, M.; Diaspro, A.; Brandi, F. Luminescent silicon nanoparticles prepared by ultra short pulsed laser ablation in liquid for imaging applications. *Opt. Mater. Express* **2012**, *2*, 510–518. [CrossRef]

20. Intartaglia, R.; Bagga, K.; Brandi, F.; Das, G.; Genovese, A.; Di Fabrizio, E.; Diaspro, A. Optical properties of femtosecond laser-synthesized silicon nanoparticles in deionized water. *J. Phys. Chem. C.* **2011**, *115*, 5102–5107. [CrossRef]

21. Zhang, D.; Gokce, B.; Barcikowski, S. Laser Synthesis and Processing of Colloids: Fundamentals and Applications. *Chem. Rev.* **2017**, *117*, 3990–4103. [CrossRef]

22. Sajti, C.L.; Sattari, R.; Chichkov, B.N.; Barcikowski, S. Gram scale synthesis of pure ceramic nanoparticles by laser ablation in liquid. *J. Phys. Chem. C.* **2013**, *114*, 2421–2427. [CrossRef]

23. Bagga, K.; McCann, R.; Wang, M.; Stalcup, A.; Vazquez, M.; Brabazon, D. Laser assisted synthesis of carbon nanoparticles with controlled viscosities for printing applications. *J. Colloid Interface Sci.* **2015**, *447*, 263–268. [CrossRef]

24. Rehbock, C.; Merk, V.; Gamrad, L.; Streubela, R.; Barcikowski, S. Size control of laser-fabricated surfactant-free gold nanoparticles with highly diluted electrolytes and their subsequent bioconjugation. *Phys. Chem. Chem. Phys.* **2013**, *15*, 3057–3067. [CrossRef]

25. Cortez-Lemus, N.A.; Licea-Claverie, A.; Paraguay-Delgado, F.; Alonso-Nuñez, G. Gold nanoparticles size design and control by poly(N,N′-diethylaminoethyl methacrylate). *J. Nanomater.* **2015**, *2015*, 273814. [CrossRef]

26. Semlali, S.; Cormary, B.; De Marco, M.L.; Majimel, J.; Saquet, A.; Coppel, Y.; Gonidec, M.; Rosa, P.; Drisko, G.L. Effect of solvent on silicon nanoparticle formation and size: A mechanistic study. *Nanoscale* **2019**, *11*, 4696–4700. [CrossRef] [PubMed]

27. Amendola, V.; Meneghetti, M. What controls the composition and the structure of nanomaterials generated by laser ablation in liquid solution? *Phys. Chem. Chem. Phys.* **2013**, *15*, 3027–3046. [CrossRef]

28.   Yang, S.; Cai, W.; Zhang, H.; Xu, X.; Zeng, H. Size and Structure Control of Si Nanoparticles by Laser Ablation in Different Liquid Media and Further Centrifugation Classification. *J. Phys. Chem. C.* **2009**, *113*, 19091–19095. [CrossRef]

29.   Bajaj, G.; Soni, R.K. Effect of liquid medium on size and shape of nanoparticles prepared by pulsed laser ablation of tin. *Appl. Phys. A.* **2009**, *97*, 481–487. [CrossRef]